Low-energy antiphase boundaries, degenerate superstructures, and phase stability in frustrated fcc Ising model and Ag-Au alloys

N. A. Zarkevich,* Teck L. Tan, L.-L. Wang, and D. D. Johnson†
Department of Materials Science and Engineering, University of Illinois, Urbana-Champaign, 61801, USA
(Received 20 July 2007; revised manuscript received 21 November 2007; published 21 April 2008)

An Ising model exhibits zero-energy antiphase boundaries (APBs) and frustration on close-packed face-centered cubic (fcc) and triangular lattices. The frustration results in degenerate structures and chains of long-period superstructures forming a quasicontinuous ground-state "hull" in the formation energy versus composition (c) diagram. In alloys, a nonzero but small APB energy yields a c-dependent reduction in this degeneracy that affects the phase diagram topology and range of the two-phase coexistence. Using density functional theory combined with cluster expansions (CEs), we study Ag-Au alloys as a prototype and find the effective cluster interactions (dominated by nearest-neighbor pairs), predict energetics of millions of structures, and construct the temperature versus c phase diagrams. We then compare the CE interactions for Ag-Au with those calculated directly from a supercell approach, and visualize the electronic origins of pair and multibody interactions, highlighting the physical nature of the chemical interactions implicit in the CE methods. We discuss generality of the results for close-packed alloys.

DOI: 10.1103/PhysRevB.77.144208 PACS number(s): 61.66.Dk, 71.20.Be, 81.30.Bx, 05.50.+q

I. INTRODUCTION

Frustrated systems are not only intriguing mathematical models, they can describe interesting physical phenomena (such as chemical or magnetic ordering) in many important materials, including alloys, magnetic systems, and superconductors.[1–16] On the other hand, (re)discovery of the chains of long-period superstructures (LPS) on the ground-state hulls in the formation energy versus concentration has attracted significant interest.[17–27] These LPS are linear combinations of the bounding, most stable stoichiometric ground states, and arise due to the limited range of interactions that do not distinguish between such structures and lead to zero-energy planar [antiphase boundary (APB)] defects.

In the present article we investigate systems with internal frustration, and show that existence of the low-energy (zero-energy) APB results in similar-energy (degenerate) structures, some of which are the ground states, while others look similar to superposition of the ground states, forming chains of LPS on the ground-state hull. An example of a frustrated system is a nearest-neighbor (NN) pair Ising model with ordering (antiferromagnetic) interactions on a close-packed triangular or face centered cubic (fcc) lattice, where the binary alloy exhibits so-called "superdegeneracy"[28–34] due to the above effects—with a narrowed $L1_2+L1_0$ coexistence region compared to a typical fcc alloy phase diagram. Because the NN pair is the dominant (strongest) interaction in most alloys and many metals have a close-packed lattices, understanding frustration in a "simple" fcc Ising model is crucial for understanding similar phenomena in real alloys, especially ones that have small, but non-negligible, multibody or longer-ranged pair interactions that alter the phase diagram topology significantly.

As a prototype of a close-packed alloy with dominant NN pair interaction, we consider fcc Ag-Au. Using density-functional theory (DFT), we calculate pair and multibody interactions in Ag-Au directly using large supercells, and show how they originate from the electronic density. We also fit the interactions to a database of many DFT structural energies using the cluster expansion (CE) method, a valuable tool for predicting alloy thermodynamics, which is used extensively.[26,27,35–56]

We compare the interactions obtained from the CE and those found directly from DFT calculations involving supercells. We also visualize the electronic density related to the effective interactions obtained from CE, demonstrating that CE interactions give physical insight, provided that a compact basis[37] is retained. We calculate the energetics of millions of structures to predict ground states and study phase stability, including how small breaking of the degeneracies (as in Ag-Au alloys) affect the phase diagrams. We use the interactions within a lattice Monte Carlo (MC) program to study thermodynamics and to construct phase diagrams. We emphasize that frustrated systems with degenerate LPS can have phase coexistence and "superdegeneracy" regions instead of phase segregation in clustering systems.

II. METHODS

We use the Vienna *ab initio* Simulation Package (VASP)[57–60] for both direct calculation of interactions, and combined with the computational Thermodynamic Tool-Kit (TTK)[61] for multiscale modeling via an optimal cluster expansion.[37] The DFT enthalpies are obtained using VASP's projector augmented-wave (PAW) basis[62,63] with the generalized-gradient approximation (GGA),[64] using the PW91 exchange-correlation functional.[64] For the Ag-Au alloy structures at various compositions, we use a 400 eV plane-wave energy cutoff and converged Brillouin zone integration meshes[65] consisting of 8^3 to 16^3 k points per cell, depending on the cell size. For a given k-mesh, with Methfessel-Paxton (or Gaussian) smearing of 0.2 eV, the energy convergence was below 1 meV/atom. All the structures are fully relaxed using the conjugate-gradient method in VASP so that pressures are below 5 kB (magnitudes of forces on each atom were below 0.02 eV/Å). The extraction of

 ©2008 The American Physical Society

TABLE I. V_{nf} (in meV) and their degeneracies D_{nf} for fits to Ag-Au using the cluster expansion with optimal set of clusters (CE), compact NN-tetrahedron only (CE-*T*), NN-pair only (CE-*P*), and NN pair and triplet restricted to structures with $0 \leq c \leq 1/4$ (CE-*R*). Interactions from DFT supercell calculations (direct) are provided also. CV1 and CV0 scores for each CE fit are given to assess errors, along with r.m.s. error between the enthalpy predictions from the direct and DFT for 55 (in parentheses, 19 of 55 for $0 \leq c \leq 1/4$) structures.

			V_{nf} (meV)				
n	f	D_{nf}	CE	CE-*T*	CE-*P*	direct	CE-*R*
0	1	1	0.64	0.18	0	−87238.23	0.4
1	1	1	−178.48	−176.58	−175.46	−659.08	−175.88
2	1	12	27.02	29.38	29.10	28.15	28.17
	2	6	0.2				
	3	24	0.3				
	4	12	0.47				
	5	24	0.34				
	6	8	−0.64				
	7	48	−0.11				
	8	6	0.36				
3	1	24	−0.48	0.04		−0.24	−0.31
	2	36	0.32				
	3	72	0.99				
4	1	8	3.45	−0.73		−1.87	
	2	48	−0.96				
	3	48	−0.86				
CV1 score			0.47	1.05	0.99		
CV0 score			0.25	0.92	0.93		0.28
r.m.s. error						3.90 (2.08)	

chemical interactions via DFT supercell calculations is discussed in Sec. II B.

An iterative procedure is used to search for the ground states and to select the 55 Ag-Au structures for DFT calculations. In the first iteration, we use the DFT enthalpies of the first 29 structures[38] having up to 4 atoms per unit cell (generated using the "smallest first" algorithm)[39,66,67] to construct the initial CE. A ground-state search over millions of possible structural configurations (with up to 20 atoms per unit cell) is conducted using the CE enthalpies. Enthalpies of any new CE-predicted ground states are then confirmed by DFT. The latter are added to the pool of DFT enthalpies to construct a new CE for the ground state search in the subsequent iteration. The above iterative process stops when the final CE does not predict any new ground states.

A. The Cluster Expansion

Although CE is broadly used[35–55] and implemented in several packages, such as ATAT[68–70,108] or TTK,[61] the various implementations differ in how they select the clusters and their weights for getting effective cluster interactions. We note that vibrational contributions can be included, as briefly discussed later, and that there are general relations between many-body potentials and the CE interactions.[71] We use the optimal CE method described in 37, which relies on a compact CE basis.

An atomic configuration (structure) σ on a lattice can be described by a set of occupational variables $\{\xi_p^\alpha\}_\sigma$, with $\xi_p^\alpha = 1$ (0) if the lattice site p is (not) occupied by an atom of type α. If every site is occupied, then $\Sigma_\alpha^{m_\alpha} \xi_p^\alpha = 1$ for every site p, where m_α is the number of atomic types ($m_\alpha = 2$ for binaries), and we need to consider only $(m_\alpha - 1)$ independent atomic types (one for binary alloys). The CE enthalpy of a configuration σ is given by

$$H(\sigma) = V_{01} + \sum_{n,f} \frac{1}{n} D_{nf} V_{nf} \bar{\Phi}_{nf}(\sigma), \tag{1}$$

where

$$\bar{\Phi}_{nf}(\sigma) = \frac{1}{N} \sum_{p_1}^{N} \xi_{p_1} \frac{1}{D_{nf}} \sum_{d}^{D_{nf}} \prod_{i=2}^{n} \xi_{p_i} \tag{2}$$

are the averaged correlation functions of n-body clusters of type f for atomic configuration σ, D_{nf} are degeneracies of the symmetry-equivalent n-body clusters $\{p_1 \cdots p_n\}_{nfd}$, and V_{nf} are interactions, see Table I. In the last product in Eq. (2), $p_i \subset \{p_1 \cdots p_n\}_{nfd}$ and $p_i \neq p_1$ for $i \geq 2$. Often it is convenient to use formation enthalpy relative to the elemental end

points. For binaries, the formation enthalpy is

$$\Delta H^F(\sigma) = H(\sigma) - [(1-c)H(0) + cH(1)]$$
$$= \sum_{n\geq 2} \sum_f \frac{1}{n} D_{nf} V_{nf} [\bar{\Phi}_{nf}(\sigma) - c], \quad (3)$$

in which only two-body and higher-order interactions determine the relative stability and ordering of the alloy.

The effective cluster interactions V_{nf} (denoted as $\tilde{V}_{nf}$ in 39) are obtained via fitting DFT enthalpies of 55 Ag-Au structures of various compositions, using a set of clusters with the smallest predictive error. The predictive error is evaluated by the leave-out-one cross-validation score (CV1),[37,68,72–75] where an upper (lower) bound on error is established by the cross-validation score of leave-out-two CV2 (leave-out-zero, CV0, i.e., least-squares) types.[39] For comparison, we also fit the same set of DFT enthalpies to other (not optimal) selected cluster sets, including NN pair only (Ising model), and compact NN clusters (pair, triplet, and quadruplet) used in the tetrahedron approximation[76–78] within the cluster variation method (CVM),[79,80] which can then be compared to the interactions determined directly.

Lattice MC simulations, as implemented within TTK,[61] are performed in periodic boxes with 16^3 (4096) to 32^3 (32768) atoms, with 4000–25000 sampling steps and 1000–16000 equilibration steps (largest values are for lowest temperatures). Phase transitions are determined from either fixed composition (variable temperature) or fixed temperature (variable chemical potential) MC runs, using plots of heat capacity versus temperature or chemical potential versus composition.

B. Extracting interactions from supercells

To calculate directly the n-body NN interactions of Au solutes in fcc Ag, we carried out DFT calculations with NN Au dimer, trimer, and tetramer on an fcc Ag lattice. A cubic cell of 32 atoms (i.e., $2\times2\times2$ fcc four-atom cells) with 8.30 Å in each dimension was used to exclude the interactions of Au atoms or clusters with their periodic images. All convergence criterion were the same as for the concentrated alloys, using an $8\times8\times8$ k-point mesh.

In this way we can calculate the DFT energies of fcc Ag $E_{(0)}$ as well as the Au monomer $E_{(1)}$, dimer $E_{(2)}$, trimer $E_{(3)}$, and tetramer $E_{(4)}$ embedded in fcc Ag. These energies can be expressed in terms of the NN ($f=1$) n-body interactions V_{n1} as follows:

$$E_{(0)} = V_{01}, \quad E_{(1)} = V_{01} + V_{11}, \quad E_{(2)} = V_{01} + 2V_{11} + V_{21},$$
$$E_{(3)} = V_{01} + 3V_{11} + 3V_{21} + V_{31},$$
$$E_{(4)} = V_{01} + 4V_{11} + 6V_{21} + 4V_{31} + V_{41}. \quad (4)$$

Conversely, the NN interactions are linear combinations of the above energies:

$$V_{01} = E_{(0)}, \quad V_{11} = -E_{(0)} + E_{(1)}, \quad V_{21} = E_{(0)} - 2E_{(1)} + E_{(2)},$$
$$V_{31} = -E_{(0)} + 3E_{(1)} - 3E_{(2)} + E_{(3)},$$
$$V_{41} = E_{(0)} - 4E_{(1)} + 6E_{(2)} - 4E_{(3)} + E_{(4)}. \quad (5)$$

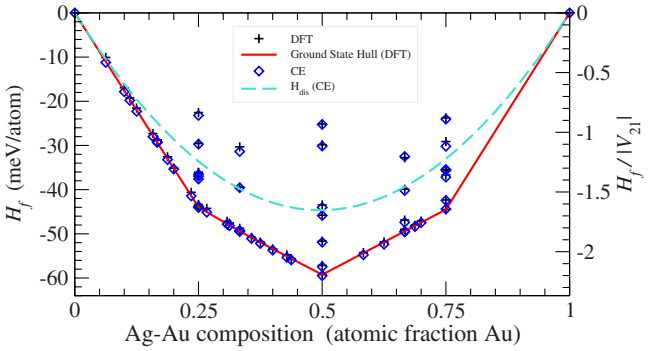

FIG. 1. (Color online) Formation enthalpies of 55 fcc Ag-Au structures from DFT (crosses) and optimal CE (diamonds), with interactions in Table I. Enthalpies for ground states [solid (red) line] and fully disordered states (dashed line) are shown.

These values represent cluster interactions at dilute concentrations of Au determined directly and can be put into Eq. (1) to predict the absolute enthalpy of a given structure. The root-mean-squared (r.m.s.) error between this prediction and DFT is shown in Table I.

III. RESULTS AND DISCUSSION

A. Ground states and effective interactions

Using the iterative procedure described in Sec. II, we find an optimal CE that accurately represents the DFT results, as shown in Fig. 1, where the CV1 score (a measure of predictive error) is 0.47 meV, and CV0 (least-squares error) is 0.28 meV. From the CE we also predict the homogeneously (fully) disordered phase and the lowest-energy structures, see Fig. 1. The latter are connected to form the ground-state "hull" of the formation enthalpy vs. composition plot (so named because it resembles the hull of a ship). The difference between ground states and fully disordered enthalpies at fixed composition determines the temperature scale of the order-disorder transition.[39] In addition, the CE permits direct prediction of millions higher-energy structures, discussed below, and shown in Fig. 2. In what follows, we use the "smallest-first" algorithm[39,66,67] for structure enumeration, see Sec. 2A in 39.

As is evident in Fig. 2(b), CE predicts that chains of structures occur on the Ag-Au ground-state hull, some of which are verified by DFT in Fig. 1. Well-distinguished ground states at $c=1/4$ (Ag_3Au), 1/2 (AgAu), and 3/4 ($AgAu_3$) are $L1_2$, $L1_0$, and $L1_2$ structures, respectively. The chains of superlattice structures (previously referred to as "adaptive" structures)[27] along the hull are created by linear combinations of smaller stoichiometric ground-state structures with low-energy APB. This results in a large number of degenerate "superstructures" at fixed composition. In addition, when the APB costs exactly zero energy, an infinite number of degenerate states occur, called superdegeneracy in the Ising model.[28–30,33,34]

We find that there is a very small (below 1 meV/atom) energy difference between structure No. 2 ($L1_0$-AgAu) and structures No. 434, 1643, 1644, 8135, and 8375 at $c=1/2$;

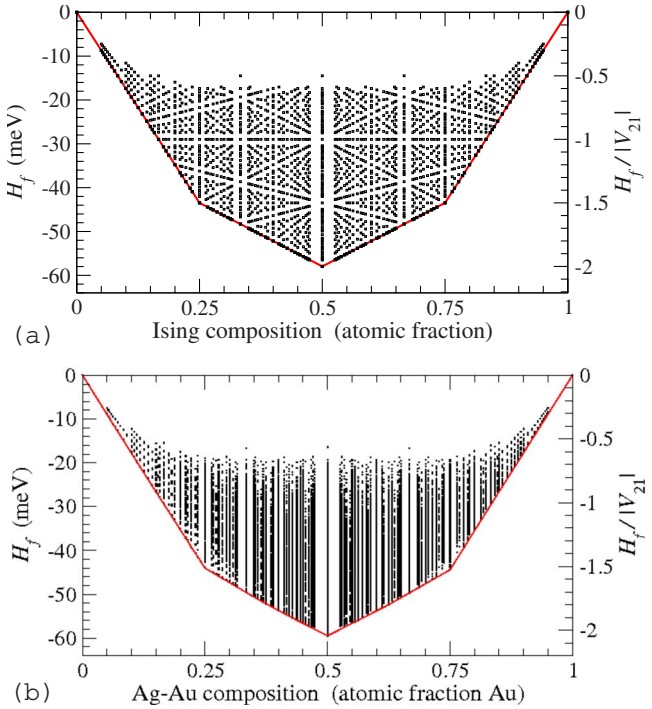

FIG. 2. (Color online) Structural formation enthalpies for cells up to 20 atoms: (a) fcc Ising model and (b) Ag-Au alloy from an optimal CE. Lines (red) are the ground-state hulls.

between No. 10 ($L1_2$-Ag_3Au) and LPS No. 12 (DO_{22}), 425, 8074, 8321 at $c=1/4$; and between No. 11 ($L1_2$-$AgAu_3$), 437 and 8388 at $c=3/4$. Such small energy differences between the ground states and competing structures are due to the low APB energies and allow formation of the chains of LPS on or near the ground-state hull, see Fig. 2.

Being a feature of the frustrated (zero-energy APB) fcc Ising model,[31,32] such LPS chains on the ground-state hull are also expected to form in any fcc alloys with dominant NN interactions; Ag-Au is only one example of such alloys.[81–85] In particular, $hP6$ structure (space group $P6/mmm$, No. 191) at $c=1/6$ can be viewed as a linear combination of $L1_2$ at $c=1/4$ and $A1$ at $c=0$; hence, it is located on the line connecting those ground states. A nonzero APB energy from longer-range interactions introduces a curvature to this line of LPS, either removing them from the ground-state hull or forming chains of new ground states with a positive curvature. For example, Ag-Au does not have ground states at $3/4<c<1$ in Fig. 1, but has many structures on the ground-state hull at compositions $0\leq c\leq 3/4$. Similar "adaptive" structures are also predicted for the fcc Cu-Au and Ni-Pt alloys.[27] We emphasize that the NN-pair interaction is dominant in most alloys, and many metallic alloys have close-packed fcc or hcp lattices; hence, there are many alloys exhibiting chains of structures on their ground-state hulls. Our results are quite general and applicable to any fcc system, which can be described as a frustrated Ising model with added longer-range perturbations. Note, however, that multibody interactions actually can screen the larger, short-ranged pair interactions, sometimes dramatically, see, e.g., 71.

Ag-Au interactions V_{nf} are displayed in Table I. For completeness, the values of V_{01} and V_{11} are reported, although they do not affect [see Eq. (3)] the ordering temperatures nor the topology of the phase diagrams. The NN pair interaction V_{21} is clearly dominant. The longer-range pair and multibody interactions in Ag-Au are small, but they are numerous and their aggregated effect is not negligible. For example, a restricted CE using only NN tetrahedron (and its subclusters) has a four-body interaction that is opposite in sign to the optimal CE; this sign change depresses the transition temperature compared to the optimal CE, see Table II, and changes topology of the phase diagram. Longer-range interactions introduce nonzero energy APBs, reducing or removing degeneracy. For Ag-Au, those APB energies are small due to small interactions. Due to the compositional effect, some APB energies are negative on the Ag-rich side (while they are positive on the Au-rich side), resulting in positive (negative at $c>3/4$) curvature of the chains of "adaptive" LPS (and lifting them from the ground-state hull at $3/4<c<1$), see Fig. 1. With larger longer-ranged pairs and multibody interactions the dominance of the NN pair is rapidly lost. Thus, the loss of degeneracy is important when comparing NN-only and dominant NN cases, as it changes the topology and coexistence regions of the phase diagrams.

TABLE II. Order-disorder temperatures at stoichiometric compositions for different sets of interactions fitted to Ag-Au.

	T_c (K)		
c	CE	CE-T	Ising
0.25	144	155	152
0.50	173	149	145
0.75	193	148	152

B. The fcc Ising model revisited

The fcc Ising model with a clustering (ferromagnetic) NN pair interaction results in phase segregation, with the miscibility gap having a maximum at $c=0.5$ at $k_BT_c/|V_{21}|=2.42$. Multibody interactions in phase-segregating alloys make this miscibility gap asymmetric versus composition; a rapid estimate of their transition temperatures was discussed in 39. Here we discuss the more interesting fcc ordering (antiferromagnetic) case.[31–33,77,86–89]

Structural formation enthalpies and ground states of an Ising (NN-pair only) model for ordering on fcc lattice are shown in Fig. 2(a), and its phase diagram is shown in Fig. 3(a). Although frustration and degeneracy of the fcc Ising model is well known,[28–30,34,90–95] it is worth noting that, for example, $L1_2$, DO_{22}, DO_{23} structures at $c=1/4$ or 3/4 have degenerate energies within NN-only Ising interactions since their NN environment is the same. DO_{22} or DO_{23} can sometimes (but not always)[37] be viewed as $L1_2$ with APB(001), which have zero energy within the NN interaction range. This is also true for $L1_0$ structure at $c=1/2$, which is made up of layers of (001) planes with antiferromagnetic ordering, where the antiferromagnetic layers in $L1_2$ and $L1_0$ structures can be shuffled with respect to one another without incurring any energy cost. This allows us to estimate quickly the de-

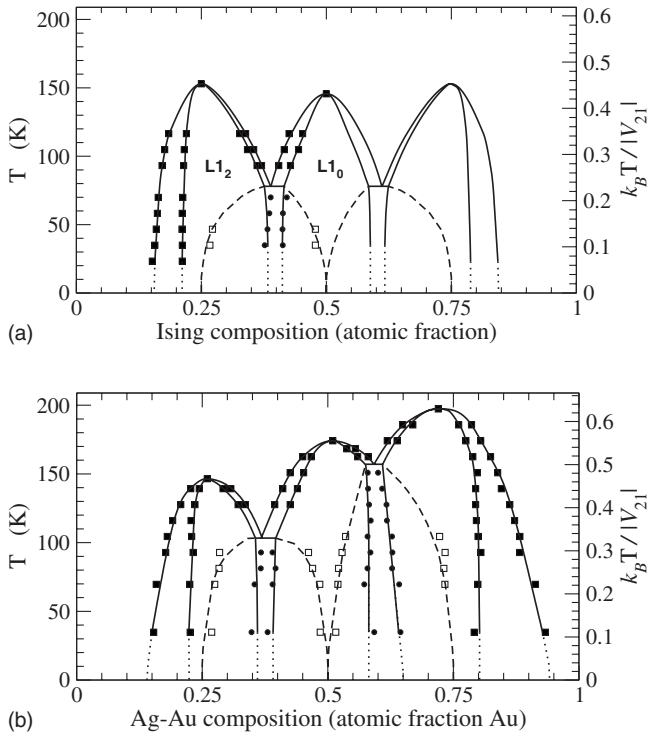

FIG. 3. T vs c phase diagram of fcc (a) Ising model and (b) Ag-Au from the optimal CE. Solid squares are determined from sharp peaks in heat capacity, with solid lines denoting boundaries. Narrow coexistence regions are below tricritical points. Other heat capacity maxima give boundaries (open squares and dashed lines) between stoichiometric phases and "superdegeneracy" regions. Dotted lines are extensions of boundaries to 0 K.

generacy in a $4L^3$-atom cell, where L^3 is the number of four-atom fcc unit cell. Accounting for cubic symmetry, the degeneracies are 2^L and 2^{2L} for $c=1/4$ (or 3/4) and $c=1/2$, respectively.[29,34]

As noted above, combining the neighboring ground states (e.g., $L1_0$ and $L1_2$, or $L1_2$ and pure elements) into larger structures with zero-energy APB yields chains of structures on the ground-state hull, see Fig. 2(a). Again, due to the numerous possible superlattice ("adaptive") structures that can be constructed from zero-energy APB configurations, there is a larger number of degenerate structures (or superdegeneracy[28–30,33,34]) as a result of a limited interaction range. Even small longer-range interactions are sufficient to reduce or remove degeneracies, giving an obvious difference between highly-degenerate Ising model and Ag-Au, see Fig. 2.

Depending on the range of interactions considered, it is possible to obtain 3 039 674 configurations with up to 20-atom unit cell.[27] In particular, for our optimal CE for the real Ag-Au involving eight pairs, three triplets, and three quadruplets (Table I), there are 1 927 602 structures that are distinguishable—with 6627 of them on the hull. In contrast, in Fig. 2(a) only 1843 structures with different energies and compositions are distinguished by the NN-pair Ising model—with 127 on the ground-state hull. Using $L=(20/4)^{1/3}$ one can estimate the degeneracies at $c=1/4$ (3/4) and 1/2 to be 3 and 11, respectively, comparing well with our actual numbers of 5 and 11. This degeneracy is much smaller than that arising from superdegeneracy, which accounts for the other 6604 degenerate structures on the ground-state hull (with two elemental states removed). Longer-range interactions in alloys lead to nonzero APB energies and (eventually) remove this degeneracy, see, e.g., Fig. 2(b) for Ag-Au.

C. Phase diagrams

Each distinguishable ground state at $c=1/4$, 1/2, and 3/4 in Fig. 2 corresponds to an ordered phase in the phase diagram in Fig. 3. At dilute concentrations a short-ranged repulsion between the solute atoms prevents them from being nearest neighbors; however, in the fcc Ising model all atomic arrangements (ordered or disordered) without NN interactions are equally energetically favored. Hence, it is not surprising that there are no finite-T phase boundaries near $c=0$ or 1.

Typically, in phase diagrams with similar topologies, the low-T region at $1/4<c<1/2$ should be a phase-segregation region. For the fcc Ising model this region is that of phase coexistence (with zero-energy APB), see Fig. 3, and is much narrower (due to superdegeneracy) than would be found for the case of less dominant NN pair interaction. Existence of zero- or low-energy APB leads to a large statistical ensemble that makes determining ordered phase boundaries at very low T difficult. Indeed, this had led to controversies in previous works on fcc Ising model, such as existence of the L' phase in CVM calculations[96] and the location of triple points in MC calculations.[29,30,33]

To identify phase transitions within MC simulations, C_v vs T and μ vs c are examined at fixed c and fixed T, respectively. At low-T, $\mu(T)$ vs c plots are used in conjunction with c_V vs T to determine coexistence regions. For the Ising model, our values of $k_BT_c/|V_{21}|$ at $c=0.25$ (or 0.75) and 0.5 are 0.45 and 0.43, respectively, in good agreement with reported values[29,30,33] of 0.46 and 0.43. (Note that the critical temperature for ordering is a factor of five times smaller than segregation and, just as with ours, published Ising phase diagrams typically do not report temperatures below $k_BT/|V_{21}|<0.1$ due to slow equilibration. Due to slow kinetics, experiments do not access these temperature anyway.) In addition, we find a triple point at $k_BT/|V_{21}|=0.23$ at $c=0.39$ (or 0.61), see Fig. 3, in agreement with MC simulation using grand canonical[30] ($c=0.39$, $k_BT/|V_{21}|=0.25$) or careful large cells[34] ($c=0.39$, $k_BT/|V_{21}|=0.245$). Importantly, only the states occurring at the vertices of the ground-state hull ($c=1/4,1/2,3/4$) have corresponding high-T phases, i.e., no LPS (or adaptive structures) that are linear combinations of those ground states.

Along with the calculated high-T boundaries (solid lines and symbols in Fig. 3), we find a narrowing of the phase coexistence due to superdegeneracy (just below the triple points), as identified earlier.[28–34] For cases where the transitions are weak and/or temperatures are low, features could not always be clearly identified from heat capacity alone; hence, we examined $\mu(T)$ vs c plots for discontinuities in the gradient. In addition, we find other maxima in the heat capacity (identified by the open squares and dashed lines) that

can become the stable coexistence boundaries if superdegeneracy is lifted among the LPS arising from stronger, longer-ranged pairs, and/or larger multibody interactions.

For NN pairs only, the phase diagram is symmetric versus composition. The multibody interactions in Ag-Au result in asymmetry of the phase diagram, see Fig. 3, and the corresponding transition temperatures, see Table II. In addition to this asymmetry, phase diagrams of fcc alloys with dominant NN interactions have similar topology to that of an Ising model, as is evident in Fig. 3. The removal of degeneracy leads to new states and raises the transition temperatures from 0 K to a low, but finite value. At low temperatures ($k_BT/|V_{21}|<0.1$), transition boundaries are difficult to determine among degenerate (or nearly degenerate) LPS so they are sometimes reported as boundaries that resemble "elephant's feet."[97] Due to vanishing kinetics at such low temperatures we do not expect those phase transitions to be observed experimentally. Importantly, low-energy structures competing with the ground states influence ordering and atomic structure of materials, affecting their properties. As the multibodies become more significant relative to the NN pair and the APB energies increase, the degeneracies are lost and the diagram no longer has the "superdegeneracy" regions (with multitudes of similar-energy superdegenerate structures) with a narrow gap (coexistence region), but the boundaries of a phase-segregation region resemble the dashed lines shown in Fig. 3. Multibodies can screen pair interactions, decreasing them by over 70%.[71]

For completeness, we note that, in general, the vibrational entropy contributions to an order-disorder temperatures can be significant. Vibrational effects add a higher level of complexity and computational difficulty, more than the CE. It can be shown (e.g., see 43 or 98) that T_c is altered by changes in harmonic vibrational entropy $\Delta S_{\text{vibr}}^{\alpha\rightarrow\beta}$ from the $\alpha-\beta$ transition from solely configurational contributions $T_{c,\text{conf}}^{\alpha\rightarrow\beta}$ as

$$T_c^{\alpha\rightarrow\beta} \approx T_{c,\text{conf}}^{\alpha\rightarrow\beta}\left(1+\frac{\Delta S_{\text{vibr}}^{\alpha\rightarrow\beta}}{\Delta S_{\text{conf}}^{\alpha\rightarrow\beta}}\right)^{-1}. \quad (6)$$

As we recently discussed in detail,[39] the importance of $\Delta S_{\text{vibr}}^{\alpha\rightarrow\beta}$ can be accurately estimated from only differences in electronegativities of solute and host. For Pd-Rh, for example, the electronegativity difference ($|0.08|$) is very small and vibrations can be ignored in determining the miscibility gap, whereas, for other systems, this estimate brings the CE T_c in agreement with experiment.[39] For Ag-Au, the electronegativities are 1.93 for Ag and 2.4 for Au, hence, not negligible. We estimate a 13% decrease (18% increase) in T_c (Table II) at Ag_3Au (at $AgAu_3$), which increase slightly the phase diagram asymmetry. The effect of vibrations should be considered for each case, but does not affect our findings generally.

D. Electronic origins of interactions

And now to the most significant point of the paper. As described in Sec. II B, using supercell techniques the local dominant NN multibody interactions can be extracted. (In principle, a transferable set of interactions, applicable to any structural configuration, can be calculated this way,[71] but the cost of computation increases exponentially with the size of the multibody cluster.) We calculated the DFT energies of pure fcc Ag $E_{(0)}$ and Au monomer $E_{(1)}$, dimer $E_{(2)}$, trimer $E_{(3)}$, and tetramer $E_{(4)}$ embedded in Ag. With these energies the NN n-body interactions V_{n1} from Eq. (5) can be ascertained directly for the dilute-Au case (i.e., 1–4 Au sites out of 32). The results of the direct calculations of interactions are listed in Table I. They are in reasonable agreement with the data from an optimal CE. However, as expected, they are in even better agreement (see Table I) with a CE restricted to the NN tetrahedron (CE-T) with all its subclusters. Both for the direct and CE-T, Table I shows that the dominant interaction is the NN pair, and that NN four-body is larger than NN three-body interaction.

We should expect a difference between interactions found from the CE using data from concentrated alloys and those found directly from the supercell with dilute concentrations of Au in Ag. In particular, the four-body tetrahedron could be less significant in the concentrated alloys as it favors segregation. So, we performed a CE fit (CE-R in Table I) using the restriction to NN pair and triplet interactions in the range of $0\leq c\leq 1/4$; these CE-R interactions are in excellent agreement with those determined directly. (The CE requires that enough structures have been calculated using DFT that contain the relevant clusters, such as three-body, in order to extract a value without infinite CV scores; hence the restriction to only NN pairs and triplets here.)

Finally, we used these direct interactions in Table I to predict the 55 structural enthalpies calculated within DFT; these and their r.m.s. error with the DFT enthalpies are given in Table I, along with r.m.s. error for the 19 out of 55 in the range of $0\leq c\leq 1/4$ (shown in parenthesis). Evidently, the direct interaction "predict" the structural enthalpies better in the restricted range (r.m.s. of ± 2 meV) where they were fit, as they better reflect the physics in that range, than they do for all 55 structures (r.m.s. of ± 4 meV—or about 46 K).

It is important to point out that "inverse" methods such as the cluster expansion[35,36,40–42,97,99–101] and "direct" methods, such as the supercells or coherent potential approximation based approaches such as concentration functionals[102] or the generalized perturbation method,[97,103–105] have been compared many times before (e.g., 106 or 107). Direct methods are directly connected to the electronic effects and have direct physical interpretation (effective interactions are related to moments of the density of states or convolutions of the electronic structure), whereas inverse CE methods, while often argued as unique, can loose the physical correctness if the basis sets are not chosen correctly,[37] including having nonunique interactions sets and no direct physical interpretation.[56]

From supercells the electronic density differences can be calculated similarly to the energy differences in Eq. (5), and the NN interactions can be visualized, see Fig. 4, with panels (a), (c), and (f) corresponding to interaction V_{21}, V_{31}, and V_{41}, respectively. We also visualize electronic density differences corresponding to

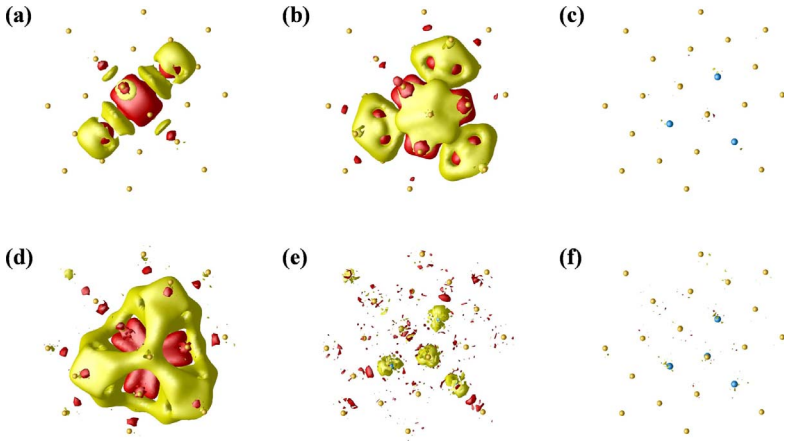

FIG. 4. (Color online) Electron density differences associated with the NN interactions for Au solutes (blue spheres) in fcc Ag (yellow spheres), viewed along [111]. Isosurfaces are plotted at $\pm 0.0003\ e/\text{Å}^3$, with red (yellow) standing for density depletion (accumulation). The electron density differences in (a), (c), and (f) correspond to the NN interactions V_{21}, V_{31}, and V_{41}, respectively, in Eq. (5). Differences (b), (d), and (e), defined in Eq. (7), show contributions of the subclusters.

$$\Delta E_3^{(1)} = V_{31} + 3V_{21} = E_{(3)} - 3E_{(1)} + 2E_{(0)},$$
$$\Delta E_4^{(1)} = V_{41} + 4V_{31} + 6V_{21} = E_{(4)} - 4E_{(1)} + 3E_{(0)},$$
$$\Delta E_4^{(2)} = V_{41} + 4V_{31} = E_{(4)} - 6E_{(2)} + 8E_{(1)} - 3E_{(0)}. \quad (7)$$

As shown in Fig. 4, for a NN Au dimer, the bonding is achieved by accumulating electron density around Au atoms and at the same time depleting it in the middle (compared to those originally associated with a monomer, i.e., a single Au impurity embedded in Ag). The same feature is evident in (b) and (d), by only subtracting contributions of Au monomers for Au trimer and tetramer, respectively. By subtracting contributions of both Au monomers and dimers from Au trimer, we get the electron redistribution associated with the direct three-body NN interaction, which is very small as shown in (c); it is even smaller than the direct four-body NN interaction shown in (f). In (e), for Au tetramer, the electron density difference corresponding to the multibody interactions beyond NN pair has the pattern of accumulating density on each Au atom and also in the interstitial tetrahedral site. Isosurfaces taken at $\pm 0.0001\ e/\text{Å}^3$ (not shown) have been checked to identify that this pattern is indeed mostly due to the three-body interaction, in accord with Eq. (7). The electron density redistribution is a direct way to illustrate the relative strength of multibody NN interactions and give the same trends observed in the data listed in Table I by both CE and direct calculations. This visualization highlights the physical origin of the cluster interactions within alloys, which are described accurately by a CE with complete and compact basis.[37]

IV. CONCLUSIONS

We considered enthalpic (structural formation versus composition c) and thermodynamic properties (T_c vs c phase diagrams) of the fcc Ising model and close-packed alloys with dominant nearest-neighbor (NN) pair interactions, exemplified by fcc Ag-Au, although this is but one example of such alloys.[81–85] We discussed degeneracy, showcased how frustration and limited interaction range introduce zero-energy antiphase boundaries (APBs), illustrated formation of the chains of long-period superstructures (LPSs) on the ground-state hull, and explained that longer-range interactions change APB energy and curvature of the LPS chains in a composition-dependent manner. We described how longer-ranged pairs or larger multibody interactions change the phase diagram and the phase-coexistence regions, widening as the dominance of the NN pair interactions is lost. Low-energy APB and LPS chains are expected to be a generic feature of the close-packed fcc alloys with dominant NN interactions. Finally, we found the interactions directly by a supercell method, confirming the dominance of the NN pair in Ag-Au, as predicted by a CE with a complete and compact basis, and showed when and how well the direct and CE interactions agree. We then visualized the electronic origins of direct chemical interactions in Ag-Au, highlighting the physical origin of the effective chemical interactions derived from direct and cluster expansion methods.

ACKNOWLEDGMENTS

We acknowledge support from the NSF by Grant No. DMR-03-12448 (D.D.J. and T.L.T.) and from the CSE Program at Illinois (T.L.T.); and support by the U.S. DOE under Sandia Metal-Hydride Center of Excellence Grant No. DEFC36-05G015064 (N.Z.), and BES Grant Nos. DEFG02-03ER15476 (L-L.W.) and DEFG02-03ER46026 (N.Z.), administered by The Frederick Seitz Materials Research Laboratory at the University of Illinois (Grant No. DEFG02-91ER45439). We acknowledge computational support by Grant Nos. DMR-0325939 through the Materials Computation Center and DMR-060017N through NCSA.

*zarkevic@ucdavis.edu
†duanej@uiuc.edu

[1] I. S. Hagemann, Q. Huang, X. P. A. Gao, A. P. Ramirez, and R. J. Cava, Phys. Rev. Lett. **86**, 894 (2001).
[2] C. Rossel, Y. Maeno, and I. Morgenstern, Phys. Rev. Lett. **62**, 681 (1989).
[3] S. R. McKay, A. N. Berker, and S. Kirkpatrick, Phys. Rev. Lett. **48**, 767 (1982).
[4] B. Pannetier, J. Chaussy, R. Rammal, and J. C. Villegier, Phys. Rev. Lett. **53**, 1845 (1984).
[5] A. J. Bray and M. A. Moore, Phys. Rev. Lett. **58**, 57 (1987).
[6] P. Chandra, P. Coleman, and A. I. Larkin, Phys. Rev. Lett. **64**, 88 (1990).
[7] A. P. Ramirez, G. P. Espinosa, and A. S. Cooper, Phys. Rev. Lett. **64**, 2070 (1990).
[8] C. M. Newman and D. L. Stein, Phys. Rev. Lett. **72**, 2286 (1994).
[9] P. Schiffer, A. P. Ramirez, D. A. Huse, P. L. Gammel, U. Yaron, D. J. Bishop, and A. J. Valentino, Phys. Rev. Lett. **74**, 2379 (1995).
[10] M. V. Feigelman and L. B. Ioffe, Phys. Rev. Lett. **74**, 3447 (1995).
[11] P. Chandra, L. B. Ioffe, and D. Sherrington, Phys. Rev. Lett. **75**, 713 (1995).
[12] M. J. Harris, S. T. Bramwell, D. F. McMorrow, T. Zeiske, and K. W. Godfrey, Phys. Rev. Lett. **79**, 2554 (1997).
[13] S. I. Matveenko and S. I. Mukhin, Phys. Rev. Lett. **84**, 6066 (2000).
[14] M. García-Hernández, J. L. Martínez, M. J. Martínez-Lope, M. T. Casais, and J. A. Alonso, Phys. Rev. Lett. **86**, 2443 (2001).
[15] A. Keren and J. S. Gardner, Phys. Rev. Lett. **87**, 177201 (2001).
[16] F. Becca and F. Mila, Phys. Rev. Lett. **89**, 037204 (2002).
[17] G. Ceder, M. De Graef, L. Delaey, J. Kulik, and D. de Fontaine, Phys. Rev. B **39**, 381 (1989).
[18] N. M. Rosengaard and H. L. Skriver, Phys. Rev. B **49**, 14666 (1994).
[19] J. Kulik and D. de Fontaine, J. Phys C **21**, L291 (1988).
[20] D. deFontaine and J. Kulik, Acta Metall. **33**, 145 (1985).
[21] J. Kulik, S. Takeda, and D. De Fontaine, Acta Metall. **35**, 1137 (1987).
[22] D. Broddin, G. Van Tendeloo, and J. Van Landuyt, Philos. Mag. A **54**, 395 (1986).
[23] G. Ceder, D. de Fontaine, H. Dreyssé, D. M. Nicholson, G. M. Stocks, and B. L. Gyorffy, Acta Metall. Mater. **38**, 2299 (1990).
[24] T. Nakano, A. Negishi, K. Hayashi, and Y. Umakoshi, Acta Mater. **47**, 1091 (1999).
[25] M. Hirabayashi, K. Hiraga, and D. Shindo, J. Appl. Crystallogr. **14**, 169 (1981).
[26] B. D. Krack, V. Ozoliņš, M. Asta, and I. Daruka, Phys. Rev. Lett. **88**, 186101 (2002).
[27] M. Sanati, L. G. Wang, and A. Zunger, Phys. Rev. Lett. **90**, 045502 (2003).
[28] H. T. Diep, A. Ghazali, B. Berge, and P. Lallemand, Europhys. Lett. **2**, 603 (1986).
[29] J. L. Lebowitz, M. K. Phani, and D. F. Styer, J. Stat. Phys. **38**, 413 (1985).
[30] U. Gahn, J. Phys. Chem. Solids **47**, 1153 (1986).
[31] D. C. Chrzan and L. M. Falicov, Phys. Rev. B **37**, 3894 (1988).
[32] D. C. Chrzan and L. M. Falicov, Phys. Rev. B **40**, 8194 (1989).
[33] K. Binder, Phys. Rev. Lett. **45**, 811 (1980).
[34] S. Kammerer, B. Dunweg, K. Binder, and M. d'Onorio de Meo, Phys. Rev. B **53**, 2345 (1996).
[35] J. W. D. Connolly and A. R. Williams, Phys. Rev. B **27**, R5169 (1983).
[36] J.M. Sanchez, F. Ducastelle, and D. Gratias, Physica A **128**, 334 (1984).
[37] N. A. Zarkevich and D. D. Johnson, Phys. Rev. Lett. **92**, 255702 (2004).
[38] N. A. Zarkevich, Complexity **11**, 36 (2006).
[39] N. A. Zarkevich, L. Teck Tan, and D. D. Johnson, Phys. Rev. B **75**, 104203 (2007).
[40] M. Asta, C. Wolverton, D. de Fontaine, and H. Dreyssé, Phys. Rev. B **44**, 4907 (1991).
[41] C. Wolverton, M. Asta, H. Dreyssé, and D. de Fontaine, Phys. Rev. B **44**, 4914 (1991).
[42] J. M. Sanchez, Phys. Rev. B **48**, 14013 (1993).
[43] A. van de Walle and G. Ceder, Rev. Mod. Phys. **74**, 11 (2002).
[44] S. V. Barabash, V. Blum, S. Muller, and A. Zunger, Phys. Rev. B **74**, 035108 (2006).
[45] V. Vaithyanathan, C. Wolverton, and L. Q. Chen, Phys. Rev. Lett. **88**, 125503 (2002).
[46] C. Wolverton and V. Ozoliņš, Phys. Rev. Lett. **86**, 5518 (2001).
[47] N. A. Zarkevich and D. D. Johnson, Phys. Rev. B **67**, 064104 (2003).
[48] N. A. Zarkevich, D. D. Johnson, and A. V. Smirnov, Acta Mater. **50**, 2443 (2002).
[49] V. Ozoliņš and M. Asta, Phys. Rev. Lett. **86**, 448 (2001).
[50] A. Van der Ven, G. Ceder, M. Asta, and P. D. Tepesch, Phys. Rev. B **64**, 184307 (2001).
[51] R. Drautz, H. Reichert, M. Fahnle, H. Dosch, and J. M. Sanchez, Phys. Rev. Lett. **87**, 236102 (2001).
[52] G. L. W. Hart and A. Zunger, Phys. Rev. Lett. **87**, 275508 (2001).
[53] S. Müller and A. Zunger, Phys. Rev. Lett. **87**, 165502 (2001).
[54] N. A. Zarkevich and D. D. Johnson, Surf. Sci. Lett. **591**, L292 (2005).
[55] G. J. Xu, N. A. Zarkevich, A. Agrawal, A. W. Signor, B. R. Trenhaile, D. D. Johnson, and J. H. Weaver, Phys. Rev. B **71**, 115332 (2005).
[56] G. L. W. Hart, V. Blum, M. J. Walorski, and A. Zunger, Nat. Mater. **4**, 391 (2005).
[57] G. Kresse and J. Hafner, Phys. Rev. B **47**, R558 (1993).
[58] G. Kresse, Ph.D. thesis, Technische Universität Wien (1993).
[59] G. Kresse and J. Furthmüller, Comput. Mater. Sci. **6**, 15 (1996).
[60] G. Kresse and J. Furthmüller, Phys. Rev. B **54**, 11169 (1996).
[61] N. A. Zarkevich, Teck L. Tan, and D.D. Johnson (unpublished).
[62] P. E. Blöchl, Phys. Rev. B **50**, 17953 (1994).
[63] G. Kresse and D. Joubert, Phys. Rev. B **59**, 1758 (1999).
[64] J. P. Perdew and Y. Wang, Phys. Rev. B **45**, 13244 (1992).
[65] H. J. Monkhorst and J. D. Pack, Phys. Rev. B **13**, 5188 (1976).
[66] A. van de Walle (private communication).
[67] L. G. Ferreira, S. H. Wei, and A. Zunger, Int. J. Supercomput. Appl. **5**, 34 (1991).
[68] A. van de Walle and G. Ceder, J. Phase Equilib. **23**, 348 (2002).
[69] A. van de Walle and M. Asta, Model. Simul. Mater. Sci. Eng. **10**, 521 (2002).
[70] A. van de Walle, M. Asta, and G. Ceder, Calphad **26**, 539 (2002).
[71] R. Drautz, M. Fahnle, and J. M. Sanchez, J. Phys.: Condens. Matter **16**, 3843 (2004).

[72] M. Stone, J. R. Stat. Soc. Ser. A (Gen.) **36**, 111 (1974).
[73] D. Allen, Technometrics **16**, 125 (1974).
[74] K.-C. Li, Ann. Stat. **15**, 958 (1987).
[75] M. H. F. Sluiter, Y. Watanabe, D. de Fontaine, and Y. Kawazoe, Phys. Rev. B **53**, 6137 (1996).
[76] C. M. van Baal, Physica (Utrecht) **64**, 571 (1973).
[77] R. Kikuchi, J. Chem. Phys. **60**, 1071 (1974).
[78] R. Kikuchi, J. M. Sanchez, D. de Fontaine, and H. Yamauchi, Acta Metall. **28**, 651 (1980).
[79] R. Kikuchi, Phys. Rev. **81**, 988 (1951).
[80] R. Kikuchi and K. Masuda-Jindo, Calphad **26**, 33 (2002).
[81] V. Ozoliņš, C. Wolverton, and A. Zunger, Phys. Rev. B **57**, 6427 (1998).
[82] Z. W. Lu, B. M. Klein, and A. Zunger, J. Phase Equilib. **16**, 36 (1995).
[83] Z. W. Lu, B. M. Klein, and A. Zunger, Model. Simul. Mater. Sci. Eng. **3**, 753 (1995).
[84] K. Terakura, T. Oguchi, T. Mohri, and K. Watanabe, Phys. Rev. B **35**, 2169 (1987).
[85] S. H. Wei, A. A. Mbaye, L. G. Ferreira, and A. Zunger, Phys. Rev. B **36**, 4163 (1987).
[86] J. M. Sanchez and D. de Fontaine, Phys. Rev. B **17**, 2926 (1978).
[87] D. F. Styer, M. K. Phani, and J. L. Lebowitz, Phys. Rev. B **34**, 3361 (1986).
[88] A. Finel and F. Ducastelle, Europhys. Lett. **1**, 135 (1986).
[89] H. T. Diep, A. Ghazali, B. Berge, and P. Lallemand, Europhys. Lett. **2**, 603 (1986).
[90] A. D. Beath and D. H. Ryan, Phys. Rev. B **73**, 214445 (2006).
[91] H. T. Diep and H. Kawamura, Phys. Rev. B **40**, 7019 (1989).
[92] P. Turchi, M. Sluiter, and D. de Fontaine, Phys. Rev. B **36**, 3161 (1987).
[93] J. Sadoc and R. Mosseri, *Geometrical Frustration* (Cambridge University Press, Cambridge, 1999).
[94] M. Elhajal, B. Canals, and C. Lacroix, J. Magn. Magn. Mater. **226–230**, 379 (2001).
[95] G. Ceder, G. D. Garbulsky, D. Avis, and K. Fukuda, Phys. Rev. B **49**, 1 (1994).
[96] R. Tetot, A. Finel, and F. Ducastelle, J. Stat. Phys. **61**, 121 (1990).
[97] F. Ducastelle, *Order and Phase Stability in Alloys* (North Holland, New York, 1991).
[98] G. D. Garbulsky and G. Ceder, Phys. Rev. B **49**, 6327 (1994).
[99] D. de Fontaine, Solid State Phys. **47**, 33 (1994).
[100] A. Zunger, in *Statics and Dynamics of Alloy Phase Transformations*, edited by P. Turchi and A. Gonis, Vol. 319 of NATO Advanced Studies Institute Series (Plenum, New York, 1994), p. 361.
[101] D. D. Johnson, in *Encyclopedia of Materials: Science and Technology*, edited by K. H. J. Buschow *et al.*, Vol. 6, (Elsevier, New York, 2001).
[102] B. L. Gyorffy and G. M. Stocks, Phys. Rev. Lett. **50**, 374 (1983).
[103] F. Ducastelle and F. Gautier, J. Phys. F: Met. Phys. **6**, 2039 (1976).
[104] F. Ducastelle and G. Treglia, J. Phys. F: Met. Phys. **10**, 2137 (1980).
[105] H. Dreyssé, A. Berera, L. T. Wille, and D. de Fontaine, Phys. Rev. B **39**, 2442 (1989).
[106] M. Sluiter and P. E. A. Turchi, Phys. Rev. B **40**, 11215 (1989).
[107] A. Gonis, X.-G. Zhang, A. J. Freeman, P. Turchi, G. M. Stocks, and D. M. Nicholson, Phys. Rev. B **36**, 4630 (1987).
[108] ATAT is available for download from http://www.its.caltech.edu/~avdw/atat